Hindawi Publishing Corporation
Advances in Condensed Matter Physics
Volume 2015, Article ID 797056, 9 pages
http://dx.doi.org/10.1155/2015/797056

Research Article

A Novel Orange-Red Emitting $ZnB_4O_7:Eu^{3+}$ Phosphor with Urchin-Like Nanostructure

Hom Nath Luitel,[1,2] Rumi Chand,[1] and Takanori Watari[1]

[1]*Department of Advanced Technology Fusion, Saga University, Honjo-1, Saga 840-8502, Japan*
[2]*GBRY Co. Ltd., 1-62-6-201 Higashiyama, Hirakata, Osaka 570-003, Japan*

Correspondence should be addressed to Hom Nath Luitel; mehomnath@yahoo.com and Takanori Watari; watarit@cc.saga-u.ac.jp

Received 16 April 2015; Accepted 14 June 2015

Academic Editor: David Huber

A novel phosphor, $ZnB_4O_7:Eu^{3+}$, with urchin-like structure consisting of radially arranged high density nanorods was successfully synthesized by hydrothermal process at 150°C for 24 h. The nanorods were measured from 200 to 400 nm in diameter and several μm in length. The urchins were few μm to 40 μm in diameter. The $ZnB_4O_7:Eu^{3+}$ phosphors were efficiently excited by ultraviolet (UV ~ 254 nm) to visible light of ~ 220 to 450 nm and exhibited intense orange-red emission consisting of main peaks at 590, 615, and 695 nm due to the charge transfer in the host and f → f transitions ($^5D_0$ to $^7F_{1,2,4}$) of the Eu^{3+} ions. Effect of the Eu^{3+} ions concentration on the photoluminescence (PL) emission intensity was investigated and it was found that 5 at% Eu^{3+} is the optimum concentration. Meanwhile, the concentration quenching mechanism was discussed. The key parameters, such as temperature dependent PL and CIE values of $ZnB_4O_7:Eu^{3+}$ phosphors, were studied. The $ZnB_4O_7:Eu^{3+}$ phosphor exhibited good thermal stability and better absorption cross section compared to the commercial $Y_2O_2S:Eu^{3+}$ phosphor. All these characteristics indicate that the phosphor will be a potential candidate for the UV based white LEDs.

1. Introduction

Recently, phosphors based on borates have attracted much attention due to their high stability, low synthetic temperatures, and high ultraviolet and optical damage threshold [1–4]. Borate crystals are intrinsically luminescent and show thermoluminescence and other interesting optical properties [5, 6]. Borates have been used as optical materials for second harmonic generation or mostly materials for fluorescence. Rare earth orthoborates like $LaBO_3$ and YBO_3 have been proved to be very useful host lattices for the luminescence of Eu^{3+} and Tb^{3+}. They found wide applications in various optical devices such as field emission displays, plasma display panels, and new generation Hg-free fluorescent lamps [7, 8]. For example, $YBO_3:Eu^{3+}$ and $YBO_3:Tb^{3+}$ are currently in use as red and green components in PDP television, respectively [9, 10]. However, these rare metal ions and their compounds are extremely expensive and the excitation maxima remained within the vacuum UV region which limits their applications in narrow regions [11, 12]. The emission efficiency of Eu^{3+} ions in most of the host is fairly low when the excitation occurs in the soft UV or blue energy range due to weak absorption (parity forbidden transitions) within the 4f shell [13]. However, under UV radiation, the Eu^{3+} ions exhibit good efficiency via associated host absorption (charge transfer band) or indirect excitation by the energy transfer process via the host absorption. For most of the RE-doped materials, especially glasses, this process has a low efficiency because the energy is almost completely lost in the glass host [14]. The photoluminescence efficiency in the soft UV to blue excitation range can be increased through associated host absorption and energy transfer or forced direct f → f transitions by manipulating/selecting the suitable host materials with low band gap or constructing the crystal lattice having low symmetry so that the forced electric dipole f-f transition of the Eu^{3+} ions will be pronounced.

Thus, there is worth finding cheaper phosphor materials with good optical-thermal stability and comparatively higher efficiency excited by near UV to visible light. Zn-borate and its hydrates are extensively studied material for

the flame retardant, smoke suppressants, afterglow suppressants, corrosion inhibitors, and synergistic agents [15–17]. Zinc borate is an optical-thermal stable compound and manyfold cheaper compared to the rare earth borates like La-borate or Y-borate. Further, the crystal structure of the ZnB_4O_7 consists of two BO_3 triangles and two BO_4 tetrahedra sharing a common vertex giving $[B_4O_7]^{2-}$ unit. Such units are repeated throughout the structure. Each zinc atom is surrounded by four close oxygen atoms (ZnO_4), arranged in an irregular and much distorted tetrahedron. The six O-Zn-O angles vary largely from 89.1 to 125.5 degrees [18] which is favourable condition for the low symmetry crystal to enhance the forbidden f-f transitions in Eu^{3+} ions. However, there are limited reports on the luminescence properties of zinc borates [19–21] and none of them has explored the photoluminescence of the ZnB_4O_7. Thus, in this paper we will discuss the details of Eu^{3+} emission in ZnB_4O_7.

One-dimensional nanomaterials such as nanowires, nanotubes, and nanobelts have attracted considerable attention because of their novel and useful physical properties leading to numerous potential applications in optoelectronics, displays devices, and storage devices [22–24]. Recently, we have reported flower-like microstructures of Zn-vanadates and compared photophysical and photocatalytic properties to the traditional solid state samples [25]. It is well proved that crystalline shape, size, and morphology of the materials are most important for the better properties. Thus, in the present paper, a cheap borate host (ZnB_4O_7) doped with Eu^{3+} ion was synthesized by hydrothermal method. Controlled morphology and enhanced optical properties have been discussed in detail.

2. Experimental

Zinc borate phosphors doped with trivalent europium ions were prepared by hydrothermal (HT) process. In the typical hydrothermal route, 10 mM $Zn(NO_3)_2{\cdot}5H_2O$ containing (0–20) at% Eu was prepared in distilled water by constant stirring at 80°C (0.01 moles of (Zn + Eu)). In a separate beaker, 40 mM H_3BO_3 was prepared in distilled water (0.04 moles of B). Citric acid (0.04 moles) was used as template and urea as precipitating agent (slightly excess compared to the metal ions). The pH of the resulting solution was adjusted by aqueous ammonia. 30 mL of the mixture (ratio of Zn : citric acid : B : urea equals $1:4:4:\geq 4$) was poured into a 50 mL Teflon lined stainless steel autoclave and kept at 150°C for 24 h. The solid obtained was centrifuged, washed multiple times with distilled water followed by ethanol, and dried at 120°C for 12 h. The sample was further calcined from 600 to 850°C for 12 h to get final zinc borate phosphors. Other samples with different Zn/B ratio were prepared in the similar way by changing the B equivalent keeping the constant Zn equivalent. For comparison, samples of ZnB_4O_7:Eu^{3+} were also prepared by solid state reaction method at 775°C for 12 h. In the solid state reaction method, analytic grade zinc oxide and slightly excess boric acid were mixed thoroughly with the help of ethanol in mortar and pestle, dried in air, and calcined at 775°C for 12 h with slow heating rate (1°C/min) to prevent the boric acid sublimation.

Phase identification was carried out using a Shimadzu XRD-6300 X-ray diffractometer with Cu Kα radiation. Thermogravimetric (TG) and differential thermal (DT) analyses were carried out using a SEIKO-6300 TG/DTA instrument. The morphology of the phosphor particles prepared by HT treatment and posttreated at 700°C was characterized by scanning electron microscopy (Hitachi-S3000N). Elemental analysis and mass percentage of the constituent atoms were estimated using energy dispersive spectroscopy X-ray mapping (EDX) coupled with SEM. Before SEM measurements, each sample was coated roughly 5 nm in thickness by platinum-palladium using Hitachi E-1030 ion sputter. Photoluminescence spectra (PL emission and diffuse reflectance) were recorded using USB 4000-UV-VIS fiber optic spectrometer (Ocean Optics). The PL excitation spectra and absolute quantum yield were recorded using Hamamatsu absolute quantum yield instrument and U6039-05 Ver3.4.2. For the absolute quantum yield measurement, photon count method was adopted where photons were collected from the excitation source in the blank cell. Then sample was loaded in the same cell and then the total photons which correspond to the emitted and unabsorbed excitation source photons were collected. The ratio of photon emitted by the samples to the photons absorbed by the sample gives the absolute quantum yield of the phosphor. All the measurements were carried out at room temperature unless specified.

3. Results and Discussion

X-ray diffraction patterns of the ZnB_4O_7:Eu^{3+} phosphors prepared by hydrothermal process at 150°C and postannealed at various temperatures are shown in Figure 1. The diffraction peaks are well indexed according to the JCPDS card number 37-0378 of ZnB_4O_7 phase except negligible impurities of $Zn_3(BO_3)_2$. The samples were crystallized in an orthorhombic system with space group *Pbca*. The crystal structure of the ZnB_4O_7 consists of two BO_3 triangles and two BO_4 tetrahedra sharing a common vertex giving $[B_4O_7]^{2-}$ unit. Such units are repeated throughout the structure. Each zinc atom is surrounded by four close oxygen atoms (ZnO_4), arranged in an irregular and much distorted tetrahedron. The six O-Zn-O angles vary largely from 89.1 to 125.5 degrees [18]. The Zn atom seems to be essentially covalent and tetrahedrally bonded to four oxygen atoms [18]. The cell parameters obtained from XRD results are as follows: a = 13.6 Å, b = 8.1 Å, and c = 8.6 Å, which is in good agreement with the reported data [18]. Here, doped Eu^{3+} ions are supposed to occupy Zn sites even though there is charge imbalance. Thus, two types of Eu^{3+} sites are possible in the ZnB_4O_7 matrix. However, due to bigger size of Eu^{3+} ions, it prefers the six-coordinated site assisted by interstitial oxygen atoms, which further distorts the ZnB_4O_7 crystal structures.

Figure 2 shows the TG-DTA profile of the $1ZnO : 4H_3BO_3$ mixture under the progress of firing temperature. The weight loss of ~26% in the TG curve is due to the loss of water molecules from the H_3BO_3 used in the reaction mixture. As seen from the DTA, the endothermic peaks at 123°C and 158°C, the loss of water molecules takes place in

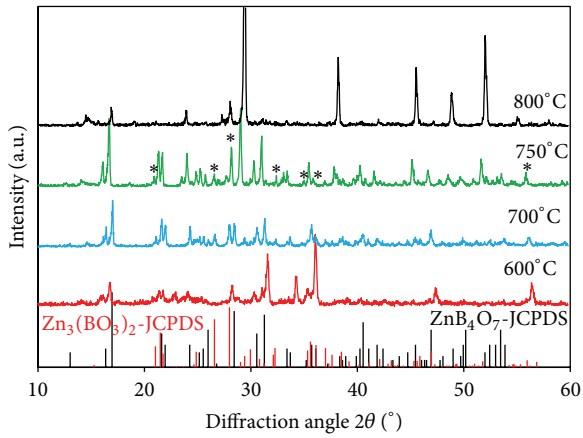

FIGURE 1: XRD patterns of ZnB_4O_7:5 at% Eu calcined at various temperatures.

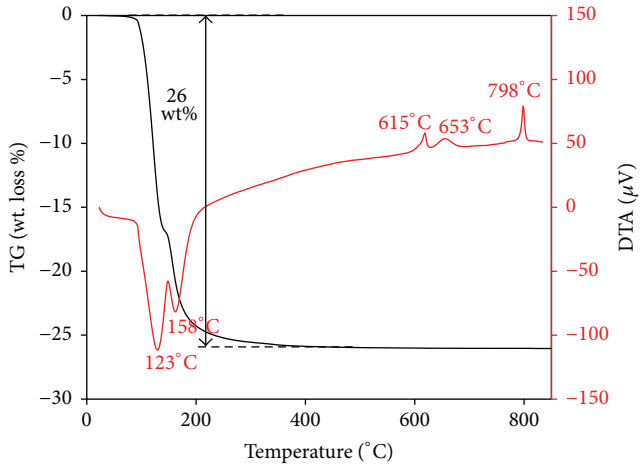

FIGURE 2: TG-DTA profile of $1ZnO : 4H_3BO_3$ mixture showing reaction progress during raising temperature.

two successive steps, one being at 123°C and the other at 158°C; both are comparatively at lower temperature than the reported data [26, 27]. Further, the exothermic peaks at 615°C and 653°C correspond to the formation of ZnB_4O_7 phase. Very sharp peak at 798°C corresponds to the phase transformation from α-ZnB_4O_7 phase to β-ZnB_2O_4 phase as observed in the XRD diagram in Figure 1. Thus, it is concluded that the α-ZnB_4O_7 phase is stable only up to 798°C in an air ambient.

The morphology and size of zinc borates phosphors were investigated by SEM micrographs. Figures 3(a)–3(d) represent the SEM image of various samples. The HT sample prepared under basic condition (pH ~ 9 using aqueous ammonia) showed urchin-like nanocluster. It is clearly observed that the cluster is composed of numerous spherical urchins of micrometer dimensions. Survey micrographs showed that over 90% of individual urchins have diameter of 15–30 μm. Each urchin is composed of radially oriented pin-like nanostructures. More careful observation of the enlarged SEM image of single urchin is shown in Figure 3(b). This image shows that the urchin is a three-dimensional, spherical, and typically 30 μm in diameter. The structures of nanostructure in a typical urchin were further studied at higher magnification SEM image and shown in Figure 3(c). It is clear that pin-like nanostructures have a regular column shape with solid structure and several micrometers in length. The diameter of the nanorod ranges within 100 nm–300 nm. Our study suggests that these pin-like nanorods are solid rather than hollow tubes. The formation mechanism of the nanorods and urchins is summarized in Figure 4 and can be explained as follows; first, zinc ions get complexes with citric acid and form zinc-citrate complex. Ion exchange followed by precipitation forms zinc borate. These zinc borates or their hydrates form crystal nucleus. Unidirectional growth of the zinc borates crystal nucleus forms nanorods during the hydrothermal treatment process due to the presence of growth directing agent, here citric acid. These nanorods aggregates are cross-linked with each other in presence of citric acid surfactant which is in excess outside the host. During the hydrothermal treatment, these nanorods get self-assembled in a radial fashion forming a spherical structure. The nanorods arrange themselves radially from the core, presumably because of the presence of excess citric acid molecule, while maintaining a constant degree of edge curvature. Numerous nanorods self-assemble into an urchin-like structure getting bigger and bigger structure. Then during the hydrothermal treatment these self-assembled structures rolled over forming smooth, dense, and ordered urchin-like structures. The growth direction of the pin-like nanostructures is radially outwards from the core of the structure. Similar urchin-like structures were explained by O'Dwyer et al. in the vanadium oxides during hydrothermal treatment containing amine surfactant [28]. A typical EDX image of the phosphor is presented in the inset of Figure 3(c) and reveals the composition of Zn, B, O, and Eu in the phosphor. Importantly, the nanostructure remained intact even after heat treatment of the phosphor materials up to 700°C. A typical SEM image of the solid state sample prepared at 775°C is presented in Figure 3(d). It is clear that the morphology of the solid state sample is irregular, composed of particles ranging from few μm to tens of μm. Irregular particles with wide size distribution are the main drawback of the solid state method.

Figure 5 shows the excitations, emissions, and UV lights irradiated optical photographs of the ZnB_4O_7:5 at% Eu^{3+} phosphor compared with the solid state sample. The excitation spectra were recorded monitoring three main emission wavelengths at 590, 615, and 695 nm, respectively. The excitation spectra exhibited a broad band in the range of 250–300 nm with a maximum around 265 nm along with several weaker excitation peaks from 310 to 450 nm. The broad band around 250–300 nm is attributed to the $O^{2-} \rightarrow Eu^{3+}$ charge transfer transition in the Eu^{3+} doped ZnB_4O_7 phosphor [29]. The main excitation peaks at 323, 375, 398, and 420 nm are assigned the $^7F_0 \rightarrow {}^5D_4$, $^7F_0 \rightarrow {}^5L_7$, $^7F_0 \rightarrow {}^5L_6$, $^7F_0 \rightarrow {}^5D_3$ transitions while the remaining weaker peaks are due to the remaining inner-shell transitions of Eu^{3+} ions [30]. Here, important point to be noted is that the excitation edge located

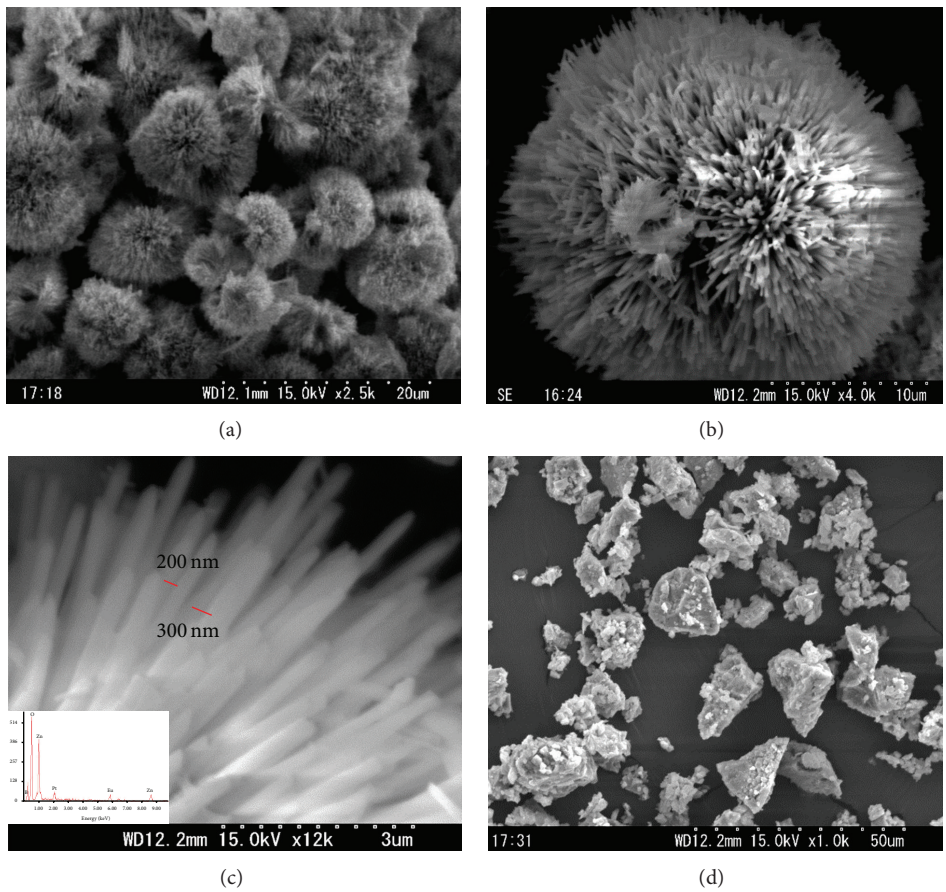

Figure 3: SEM images of ZnB_4O_7:5 at% Eu phosphors hydrothermally treated at 150°C for 24 h at pH 9 (a, b, c) and solid state sample (d). Inset in (c) shows the typical EDS spectrum.

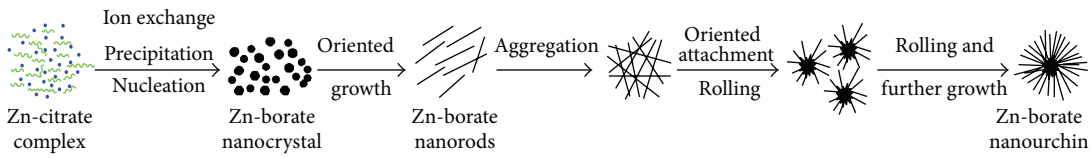

Figure 4: Schematic illustration of the formation of urchin-like ZnB_4O_7:Eu^{3+} nanostructure during the hydrothermal process.

from 380 to 410 nm (near UV to blue spectrum) is significant compared to the other Eu^{3+} doped host materials [1, 6, 10] that might be due to the highly favourable low symmetry crystal structure of borate which enhances the electric dipole intra-4f transitions. The nUV to blue edge of the excitation spectrum matches precisely with the near UV/blue LED indicating the possibility of blue LED excited white LED fabrication.

From the typical fluorescence spectra of the ZnB_4O_7:5 at% Eu^{3+} phosphor, the following emission transitions were observed and assigned the D → F transitions in the Eu^{3+} ions [31, 32]:

$$
\begin{aligned}
{}^5D_0 &\longrightarrow {}^7F_1 \quad (584 \sim 601\ \text{nm}),\\
{}^5D_0 &\longrightarrow {}^7F_2 \quad (601 \sim 627\ \text{nm}),\\
{}^5D_0 &\longrightarrow {}^7F_3 \quad (650 \sim 660\ \text{nm}),\\
{}^5D_0 &\longrightarrow {}^7F_4 \quad (687 \sim 710\ \text{nm}).
\end{aligned}
\tag{1}
$$

The main emission line near 615 nm is assigned to the Eu^{3+} electric dipole transition from the ${}^5D_0 \rightarrow {}^7F_2$ states, while the emission near 595 nm is the magnetic dipole transition from ${}^5D_0 \rightarrow {}^7F_1$. Due to the relatively high phonon energies in zinc borates, the multiphonon relaxation from higher excited level (such as ${}^5D_{1,2}$) to the ${}^5D_0$ level has a high probability and hence no emission lines from higher levels were observed [33]. The transitions are found to get split into components in the ZnB_4O_7 host. The well resolved Stark splitting (e.g., ${}^5D_0 \rightarrow {}^7F_1$ transition into three components) suggests that the Eu^{3+} ions in the hosts occupy low symmetry

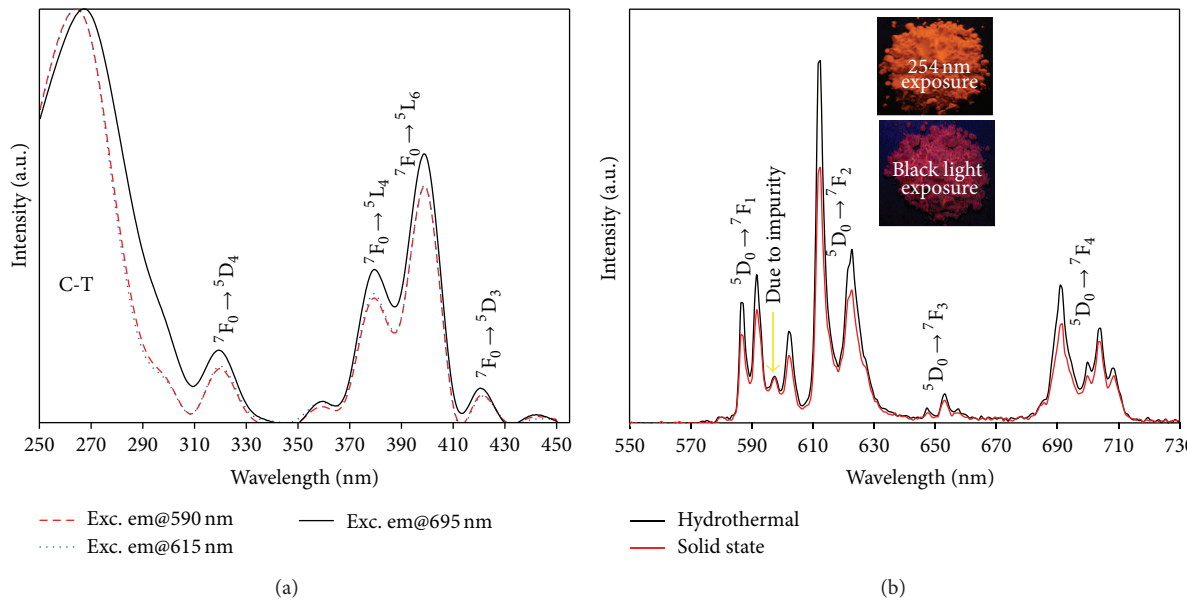

FIGURE 5: Excitation (a) and emission (b) spectra of ZnB_4O_7:5 at% Eu^{3+} phosphor. Inset in (b) is the optical photographs of the phosphor in UV and black light exposure.

sites which is very favourable condition for the forced electric dipole transition of Eu^{3+} ions [34]. As explained earlier, the bigger Eu^{3+} ions substitute smaller Zn^{2+} sites in the ZnO_4 tetrahedra; the structural distortion from regular tetrahedron occurs lowering the symmetry around Eu^{3+} ions that might be the cause of hyperfine Stark splitting into 586 m, 591 nm, and 602 nm. The other component at 597 nm is expected to originate from the Eu^{3+} ions in $Zn_3(BO_3)_2$ impurity present as seen in the XRD pattern in Figure 1 [35]. It is clear that the hydrothermal sample exhibited intense PL emission compared to the solid state sample, probably due to dense and homogenous particles formation. These phosphors exhibit orange-red emission color under black light irradiation due to stronger emission at 610~630 nm while exhibiting the orange emission under stronger UV light (e.g., 254 nm) irradiation due to two comparable emissions at 584~601 nm and 687~710 nm (spectrum is omitted). Further, the excitation wavelength dependent quantum yields of the ZnB_4O_7:5 at% Eu^{3+} phosphor at 260 nm, 320 nm, 380 nm, 400 nm, and 420 nm with 5 nm FWHM of the excitation peaks were recorded as ~60%, 20%, 65%, 75%, and 45%, respectively.

Figure 6 shows the effect of Eu^{3+} ions concentration on the fluorescence intensity of the ZnB_4O_7:x at% Eu^{3+} phosphor. Increasing doped Eu^{3+} ions concentration, the emission intensity of all the emission peaks increased gradually till 5 at% Eu^{3+} ions concentration at which the absolute quantum yield was recorded as ~75%. It should be noted that the shape and the energetic position of the emission bands did not change much with Eu^{3+} ions concentration. We measured the XRD profile of various at% Eu doped ZnB_4O_7:x at% Eu^{3+} phosphor but no other phases appeared. At a doping concentration of Eu^{3+} greater than 5 at%,

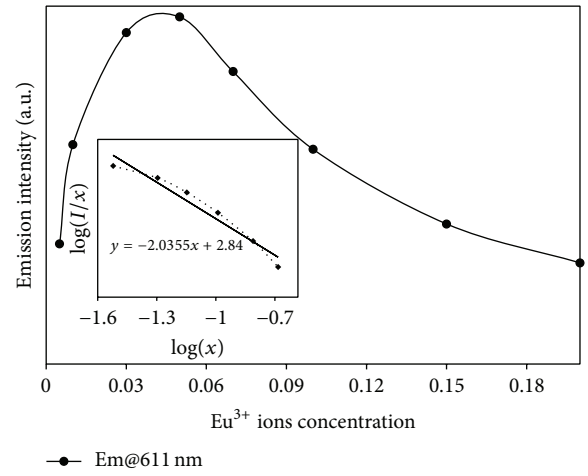

FIGURE 6: Effect of Eu^{3+} concentration on the PL emission variation of ZnB_4O_7:x at% Eu^{3+} phosphor.

the emission peaks intensities gradually decreased indicating that 5 at% Eu is the critical concentration and above that concentration quenching occurs [36]. According to Dexter theory [37], the relation between luminescent intensity "I" and activator concentration "x" can be expressed by

$$I \propto \frac{(1+A)}{\gamma\left[\alpha^{\wedge}(1-s)/3\Gamma(1+s/3)\right]}, \quad (\alpha > 1), \qquad (2)$$

where $\alpha = x[(1+A)X_0/\gamma]^{3/s}\Gamma(1-s/3) \propto x$, x is activator concentration in moles, s is series of electric multipolar, γ is intrinsic transition probability of activator, and A and X_0 are constants. There are four different quenching mechanisms,

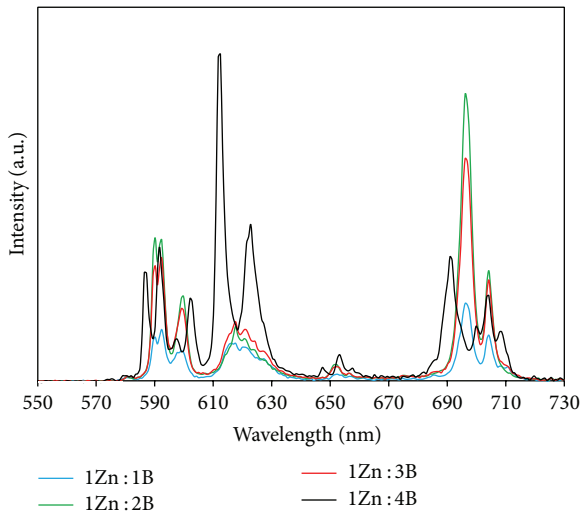

Figure 7: PL emission variation of $Zn_xB_yO_z$:5 at% Eu^{3+} phosphor with different Zn/B compositions.

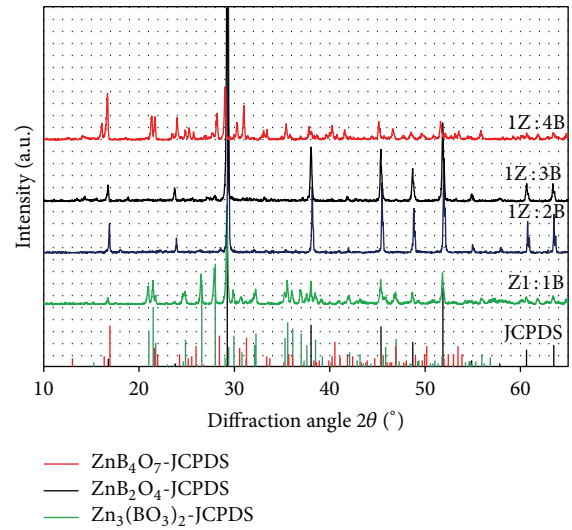

Figure 8: XRD patterns of $Zn_xB_yO_z$:5 at% Eu phosphor with different Zn/B compositions calcined at 775°C for 12 h.

that is, exchange interactions, dipole-dipole (d-d), dipole-quadrupole (d-q), and quadrupole-quadrupole (q-q) when the value of s is 3, 6, 8, and 10, respectively. If a double logarithmic relation graph between $\lg(I/x)$ and $\lg(x)$ is plotted, the slope of curve gives the type of interaction. The relation curve of $\lg(I/x)$ and $\lg(x)$ is given in the inset of Figure 6. From the inset, the value of s is 6.1065, which is very near to 6 indicating that the quenching mechanism of Eu^{3+} in ZnB_4O_7:Eu^{3+} is d-d interactions.

Figure 7 shows the effect of Zn to B composition on the PL emission characteristics. When Zn to B ratio was 1, the phosphor exhibited very low emission. When Zn to B ratio was 4, a very intense emission peak was observed consisting of major $^5D_0 \rightarrow {}^7F_2$ transition of Eu^{3+} around 611 nm in the ZnB_4O_7 host. However, if the Zn to B ratios were 2 and 3, the emission peaks at 595 nm ($^5D_0 \rightarrow {}^7F_1$ transition) and 695 nm ($^5D_0 \rightarrow {}^7F_4$ transition) were pronounced. From the XRD analysis of various Zn to B compositions presented in Figure 8, the major phase generated at Zn to B ratio of 2 and 3 was ZnB_2O_4 instead of ZnB_4O_7. It was reported that ZnB_2O_4:Eu^{3+} shows red emission with emission maximum around 595 and 695 nm [21, 38].

The CIE chromaticity coordinates of various ZnB_4O_7:Eu^{3+} phosphors excited by 255 nm UV light are presented in Figure 9. The chromaticity coordinates of 775°C and 850°C sintered phosphors are (0.544, 0.335) and (0.528, 0.338), respectively. Thus, the ZnB_4O_7:Eu^{3+} phosphor (stable below 798°C) is comparatively intense red compared to the ZnB_2O_4:Eu^{3+} phosphor (stable above 800°C, see Figure 1 for phases formed at different calcination temperatures and Figure 10 for the corresponding PL emission spectra). Figure 9 also correlates the color values of various samples with different Zn : B ratios. The color coordinates of the 1Zn : 1B, 1Zn : 2B, 1Zn : 3B, and 1Zn : 4B phosphors sintered at 775°C are (0.504, 0.311), (0.521, 0.331), (0.532, 0.351), and (0.545, 0.345), respectively. The result indicates that the color

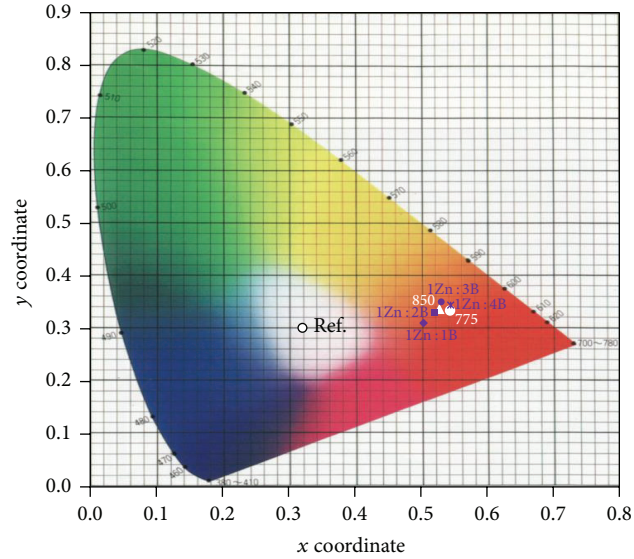

Figure 9: CIE coordinate diagram of $Zn_xB_yO_z$:5 at% Eu^{3+} phosphors.

is tunable from pure red to orange-red by the proper host composition and sintering temperature.

It is well known that with the raise of temperature the PL intensity decreased due to vibrational loss of the excited electrons. This process limits the application of phosphors at relatively hot temperatures or if the device gets heated during operation. Thus, temperature dependent emission spectra of ZnB_4O_7:Eu^{3+} phosphor were recorded and presented in Figure 11. The relative peak intensity of ZnB_4O_7:Eu^{3+} phosphor at 611 nm (the most intense emission peak) as a function of temperature was recorded and compared with the commercial Y_2O_2S:Eu^{3+} phosphor (the most intense emission peak located at 627 nm) as shown in

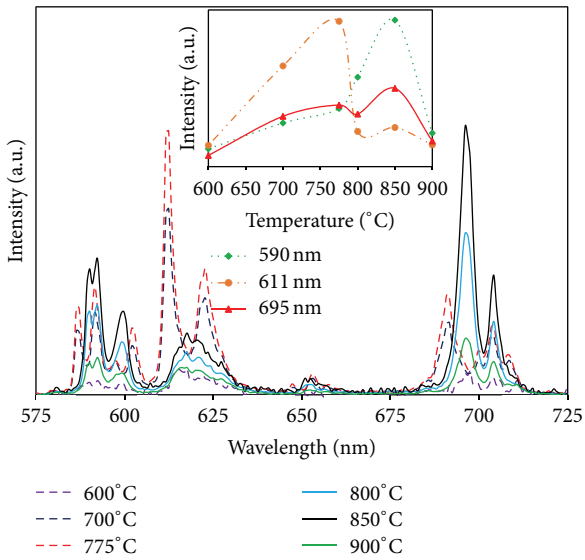

FIGURE 10: PL emission profile of ZnB_4O_7:5 at% Eu calcined at various temperatures for 12 h. Inset shows the PL emission trend of 590 nm, 611 nm, and 695 nm peaks with calcination temperatures.

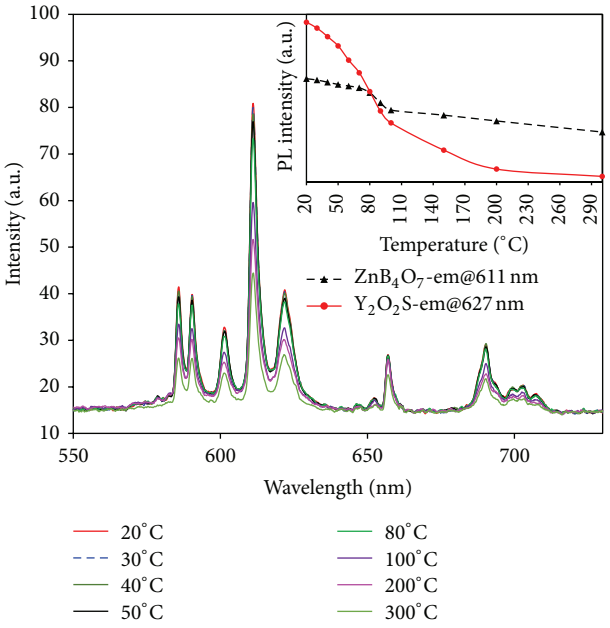

FIGURE 11: Temperature dependent emission spectra of ZnB_4O_7:5 at% Eu^{3+} phosphor. Inset is the comparison of ZnB_4O_7:5 at% Eu^{3+} (em@611 nm) with the commercial $Y_2O_2S:Eu^{3+}$ phosphor (em@ 627 nm).

the inset in Figure 11. It is clear that the emission intensity of the $ZnB_4O_7:Eu^{3+}$ phosphor decreased marginally with the raise of temperature up to 80°C above which comparatively sharp decrease was observed. However, the commercial $Y_2O_2S:Eu^{3+}$ phosphor showed sharp decrease of PL intensity at low temperatures range. It suggests that the thermal resistance of the $ZnB_4O_7:Eu^{3+}$ phosphor is very good compared to the $Y_2O_2S:Eu^{3+}$ phosphor. The relative absorption

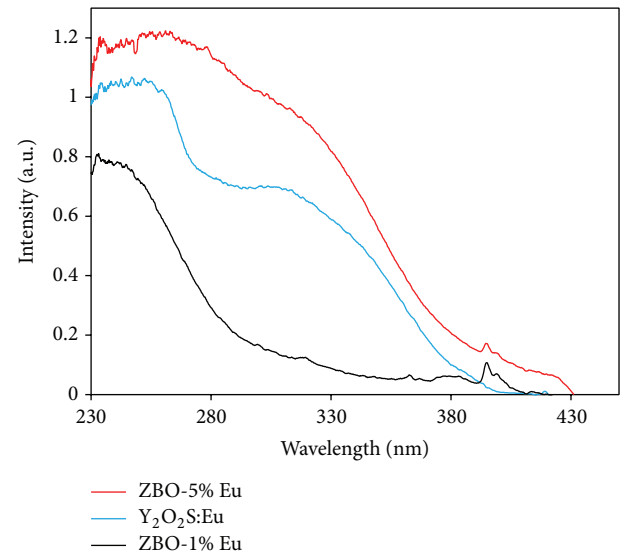

FIGURE 12: PL absorption spectra of ZnB_4O_7:Eu phosphor compared with the Y_2O_2S:Eu phosphor.

cross section experiments were carried out comparing with the commercial $Y_2O_2S:Eu^{3+}$ phosphor and the results are presented in Figure 12. It clearly suggests that $ZnB_4O_7:Eu^{3+}$ phosphor exhibited better absorption efficiency than the commercial $Y_2O_2S:Eu^{3+}$ phosphor. These phosphors have high absorbance in the UV with moderately high quantum yield (~60%), and they have potential applications in the UV excited displays and LEDs. Further, nUV to blue band absorption is also significant (about 15~20%) and comparatively higher conversion efficiencies at nUV range (~75%) suggest that the phosphor might have application in the nUV to blue LED excited white LEDs; however further improvement is needed to increase the absorption in that range.

4. Conclusions

A novel, $ZnB_4O_7:Eu^{3+}$, phosphor was successfully synthesized by hydrothermal treatment. During HT treatment, urchin-like structures consisting of radially arranged high density nanorods were formed. The nanorods were measured from 200 to 400 nm in diameter and several μm in length. The urchins were measured ranging from few μm to 40 μm in diameter. Meanwhile, the solid state samples were irregular with size of few μm to tens of micrometers. The $ZnB_4O_7:Eu^{3+}$ phosphor was efficiently excited by 250–450 nm light source and exhibited intense orange-red emission consisting of dominant peaks at 590, 615, and 695 nm due to $^5D_0 \rightarrow {}^7F_1$, $^5D_0 \rightarrow {}^7F_2$, and $^5D_0 \rightarrow {}^7F_4$ transitions of Eu^{3+} ions in the ZnB_4O_7 host. The optimum Eu^{3+} ions concentration for the best PL intensity was found to be 5 at%. The α-ZnB_4O_7 phase is stable only up to 798°C and above that temperature phase transformation to the β-ZnB_2O_4 phase occurred. The temperature dependent photoluminescence and absorption cross section results indicate that the $ZnB_4O_7:Eu^{3+}$ is a promising phosphor with good thermal stability compared

to the commercial $Y_2O_2S:Eu^{3+}$ phosphor and has a potential application in UV pumped fluorescent lamp as well as nUV to blue LED excited white LEDs.

Conflict of Interests

The authors declare that there is no conflict of interests regarding the publication of this paper.

References

[1] G. Bertrand-Chadeyron, R. Mahiou, M. El-Ghozzi, A. Arbus, D. Zambon, and J. C. Cousseins, "Luminescence of the orthoborate YBO_3: Eu^{3+}. Relationship with crystal structure," *Journal of Luminescence*, vol. 72–74, pp. 564–566, 1997.

[2] L. Lou, D. Boyer, G. Bertrand-Chadeyron, E. Bernstein, R. Mahiou, and J. Mugnier, "Sol-gel waveguide thin film of YBO_3: preparation and characterization," *Optical Materials*, vol. 15, no. 1, pp. 1–6, 2000.

[3] M. Ren, J. H. Lin, Y. Dong, L. Q. Yang, M. Z. Su, and L. P. You, "Structure and phase transition of $GdBO_3$," *Chemistry of Materials*, vol. 11, no. 6, pp. 1576–1580, 1999.

[4] R. C. Ropp, *Luminescence and the Solid State*, Elsevier, Amsterdam, The Netherlands, 2nd edition, 1991.

[5] H. Huppertz and G. Heymann, "Multianvil high-pressure/high-temperature preparation, crystal structure, and properties of the new oxoborate β-ZnB_4O_7," *Solid State Sciences*, vol. 5, no. 2, pp. 281–289, 2003.

[6] Z.-W. Zhang, X.-Y. Sun, D.-D. Jia, S.-T. Song, J.-P. Zhang, and S.-F. Wang, "Tunable full color emission from single-phase $LiSr_{3.99-x}Dy_{0.01}(BO_3)_3$:$xEu^{3+}$ phosphors," *Ceramics International*, vol. 39, no. 4, pp. 3965–3970, 2013.

[7] Z. H. Li, J. H. Zeng, C. Chen, and Y. D. Li, "Hydrothermal synthesis and luminescent properties of YBO_3:Tb^{3+} uniform ultrafine phosphor," *Journal of Crystal Growth*, vol. 286, no. 2, pp. 487–493, 2006.

[8] S. Shionoys and W. M. Yen, *Phosphor Handbook*, CRC Press, New York, NY, USA, 2nd edition, 1998.

[9] C.-H. Kim, I.-E. Kwon, C.-H. Park et al., "Phosphors for plasma display panels," *Journal of Alloys and Compounds*, vol. 311, no. 1, pp. 33–39, 2000.

[10] X. Zhang, H. Lang, and H. J. Seo, "On the luminescence of Ce^{3+}, Eu^{3+}, and Tb^{3+} in novel borate $LiSr_4(BO_3)_3$," *Journal of Fluorescence*, vol. 21, no. 3, pp. 1111–1115, 2011.

[11] Z. Yang, Y.-L. Wen, N. Sun et al., "Morphologies of $GdBO_3$:Eu^{3+} one-dimensional nanomaterials," *Journal of Alloys and Compounds*, vol. 489, no. 1, pp. L9–L12, 2011.

[12] G. Ju, Y. Hu, H. Wu et al., "A red-emitting heavy doped phosphor $Li_6Y(BO_3)_3$:Eu^{3+} for white light-emitting diodes," *Optical Materials*, vol. 33, no. 8, pp. 1297–1301, 2011.

[13] Z. Li, P. Wu, X. Jiang, Z. Zhang, and S. Xu, "The synthesis of rare earth borate glasses and their luminescence properties," *Journal of Luminescence*, vol. 40-41, pp. 135–136, 1988.

[14] G. Blasse and B. C. Grabmaier, *Luminescent Materials*, Springer, Berlin, Germany, 1994.

[15] C. Ting, D. Jian-Cheng, W. Long-Shuo, Y. Fan, and F. Gang, "Synthesis of a new netlike nano zinc borate," *Materials Letters*, vol. 62, no. 14, pp. 2057–2059, 2008.

[16] F. Samyn, S. Bourbigot, S. Duquesne, and R. Delobel, "Effect of zinc borate on the thermal degradation of ammonium polyphosphate," *Thermochimica Acta*, vol. 456, no. 2, pp. 134–144, 2007.

[17] A. Genovese and R. A. Shanks, "Structural and thermal interpretation of the synergy and interactions between the fire retardants magnesium hydroxide and zinc borate," *Polymer Degradation and Stability*, vol. 92, no. 1, pp. 2–13, 2007.

[18] M. Martinez-Ripoll, S. Martínez-Carrera, and S. García-Blanco, "The crystal structure of zinc diborate ZnB_4O_7," *Acta Crystallographica Section B Structural Crystallography and Crystal Chemistry*, vol. 27, no. 3, pp. 672–677.

[19] A. Ivankov, J. Seekamp, and W. Bauhofer, "Optical properties of Eu^{3+}-doped zinc borate glasses," *Journal of Luminescence*, vol. 121, no. 1, pp. 123–131, 2006.

[20] Y. Zheng, Y. Qu, Y. Tian et al., "Effect of Eu^{3+}-doped on the luminescence properties of zinc borate nanoparticles," *Colloids and Surfaces A: Physicochemical and Engineering Aspects*, vol. 349, no. 1–3, pp. 19–22, 2009.

[21] Z. Mu, Y. Hu, L. Chen, and X. Wang, "Enhanced red emission in ZnB_2O_4:Eu^{3+} by charge compensation," *Optical Materials*, vol. 34, no. 1, pp. 89–94, 2011.

[22] Y. Inoue, I. Noda, T. Torikai, T. Watari, T. Hotokebuchi, and M. Yada, "TiO_2 nanotube, nanowire, and rhomboid-shaped particle thin films fixed on a titanium metal plate," *Journal of Solid State Chemistry*, vol. 183, no. 1, pp. 57–64, 2010.

[23] Y. Inoue, S. Ohtsuka, T. Torikai, T. Watari, and M. Yada, "Nanostructural and morphological control of ruthenium compounds templated by surfactant assemblies," *Crystal Growth and Design*, vol. 9, no. 12, pp. 5092–5100, 2009.

[24] Y. Xia, P. Yang, Y. Sun et al., "One-dimensional nanostructures: synthesis, characterization, and applications," *Advanced Materials*, vol. 15, no. 5, pp. 353–389, 2003.

[25] H. N. Luitel, R. Chand, T. Torikai, M. Yada, and T. Watari, "Rare earth free $Zn_3V_2O_8$ phosphor with controlled microstructure and its photocatalytic activity," *International Journal of Photoenergy*, vol. 2013, Article ID 410613, 9 pages, 2013.

[26] C. E. Housecroft and A. G. Sharpe, *Inorganic Chemistry*, Prentice Hall, 3rd edition, 2008.

[27] January 2014, http://en.wikipedia.org/wiki/Boric_acid.

[28] C. O'Dwyer, D. Navas, V. Lavayen et al., "Nano-urchin: the formation and structure of high-density spherical clusters of vanadium oxide nanotubes," *Chemistry of Materials*, vol. 18, no. 13, pp. 3016–3022, 2006.

[29] D. Jin, X. Yu, X. Xu, L. Wang, L. Wang, and N. Wang, "Hydrothermal synthesis of amorphous spherical-shaped YBO_3:Eu^{3+} and its photoluminescence property," *Journal of Materials Science*, vol. 44, no. 22, pp. 6144–6148, 2009.

[30] L. Guan, Y. Wang, W. Chen et al., "Fabrication and luminescent properties of red phosphor M_3BO_6:Eu^{3+}(M=La, Y)," *Journal of Rare Earths*, vol. 28, no. 1, pp. 295–298, 2010.

[31] A. S. Souza, Y. A. R. Oliveira, and M. A. C. dos Santos, "Enhanced approach to the Eu^{3+} ion $^5D_0 \rightarrow {}^7F_0$ transition intensity," *Optical Materials*, vol. 35, no. 9, pp. 1633–1635, 2013.

[32] L. Muresan, E. J. Popovici, F. Imre-Lucaci, R. Grecu, and E. Indrea, "Studies on Y_2O_3:Eu phosphor with different particle size prepared by wet chemical method," *Journal of Alloys and Compounds*, vol. 483, no. 1-2, pp. 346–349, 2009.

[33] L. Ambrosi, M. Beitinelli, M. Ferrari, M. Casarin, and A. Piazza, "Optical spectroscopy of Eu^{3+} doped zinc borate glasses," *Journal de Physique III*, vol. 4, pp. 477–480, 1994.

[34] V. Venkatramu, P. Babu, and C. K. Jayasankar, "Fluorescence properties of Eu^{3+} ions doped borate and fluoroborate glasses

containing lithium, zinc and lead," *Spectrochimica Acta—Part A: Molecular and Biomolecular Spectroscopy*, vol. 63, no. 2, pp. 276–281, 2006.

[35] W. Zou, Z. S. Yang, M. K. Lü, F. Gu, and S. F. Wang, "Effect of Mn2+ ions on the photoluminescence characteristics of Eu^{3+}-doped $Zn_3(BO_3)_2$ nanoparticles," *Displays*, vol. 26, no. 4-5, pp. 143–146, 2005.

[36] Q. Xiao, Q. Zhou, and M. Li, "Synthesis and photoluminescence properties of Sm^{3+}-doped $CaWO_4$ nanoparticles," *Journal of Luminescence*, vol. 130, no. 6, pp. 1092–1094, 2010.

[37] D. L. Dexter and J. H. Schulman, "Theory of concentration quenching in inorganic phosphors," *The Journal of Chemical Physics*, vol. 22, no. 6, pp. 1063–1070, 1954.

[38] W.-R. Liu, C. C. Lin, Y.-C. Chiu, Y.-T. Yeh, S.-M. Jang, and R.-S. Liu, "ZnB_2O_4:Bi^{3+},Eu^{3+}: a highly efficient, red-emitting phosphor," *Optics Express*, vol. 18, no. 3, pp. 2946–2951, 2010.